Original Study **Open Access**

Katarzyna Cyran*, Michal Kowalski

Effect of pillar width on the stability of the salt cavern field for energy storage

https://doi.org/10.2478/sgem-2024-0009
received October 31, 2023; accepted May 15, 2024.

Abstract: Effective planning of the cavern field involves determining the optimal pillar width between the caverns and the feasible number of caverns based on geological and mining conditions. The proper design of the pillar width is crucial to ensure the stability of the cavern field and the rational utilization of the rock salt deposit. The stability of the pillars is a complex problem influenced by various factors, including rock salt creep, changes in the cavern pressure during operational cycles, mechanical parameters, and failure criteria of the rock salt. To address this problem, the stability of the cavern field in relation to the number of caverns and pillar widths is evaluated. The evaluation is based on the following criteria: displacements, von Mises stress, strength/stress ratio, and safety factor. Three variations of pillar width and three variants of cavern fields, differing in the number of caverns, are considered. Results show that the allowable pillar width is affected by the number of caverns in the cavern field. Moreover, the stability analysis reveals uneven stress and deformation distribution in the cavern field. When the pillar width is 2.0–3.0 times the diameter of a cavern, pillars at the centre exhibit poorer stability than those at the edges of the cavern field. However, with a narrower pillar width, the highest displacements occur at the field's edges. The findings of this study provide a valuable date in the planning, design, and operation of new cavern fields for the underground storage of energy sources such as oil, natural gas, hydrogen, and compressed air in rock salt deposits.

Keywords: salt caverns for energy storage; efficient pillar width; rational planning of cavern field; stability of cavern field; safety of storage operation.

***Corresponding author: Katarzyna Cyran,** Faculty of Civil Engineering and Recourse Management, AGH University of Krakow, Al. Mickiewicza 30, 30-059 Cracow, Poland, E-mail: kcyran@agh.edu.pl
Michal Kowalski, Faculty of Civil Engineering and Recourse Management, AGH University of Krakow, Al. Mickiewicza 30, 30-059 Cracow, Poland

1 Introduction

Salt caverns play an increasingly important role in energy storage, contributing to the maintenance of energy consumption. The underground storage of natural gas, oil, hydrogen, or compressed air in salt caverns offers numerous advantages. These caverns provide large storage capacity, safety, extended operation time, and flexibility in operation cycles. Rock salt formations are highly suitable for storage due to their remarkably low permeability and self-healing properties. With the growing demand for salt caverns, efficient utilization of rock salt resources and ensuring cavern safety become crucial considerations.

An efficient pillar design is a key objective in the planning and constructing of salt cavern facilities. This design ensures the safety of storage operations and the rational use of rock salt deposits. A salt cavern facility consists of multiple individual caverns, which are adjacent to each other and separated by pillars. The pillars are rock salt parts left between adjacent caverns to prevent their mutual influence and potential damage. Therefore, a comprehensive design of pillar width is essential for maintaining cavern stability and integrity. The pillars are influenced by various factors, including creep, changes in the cavern pressure during operation cycles, and physico-mechanical parameters of rock salt and surrounding rocks.

If the pillar width is too small, it can lead to a hydraulic connection between caverns or even failure of the pillar or caverns themselves. On the other hand, if the pillar width is too wide, it becomes uneconomical to manage the salt deposit, resulting in the wastage of salt resources. Therefore, striking the right balance in the pillar design is critical for ensuring the efficiency and sustainability of salt cavern facilities.

A considerable number of studies have been conducted to investigate the width, stability, and safety of pillars in salt mines, as reported in the works by Aubertin et al. (2018), Baryakh et al. (2015), Frayne et al. (2001), Qin et al. (2020), Swift et al. (2005), Van Sambeek (1997), among others. The design and safety of pillars in the context of underground storage in salt deposits were

mainly considered in the papers related to salt cavern stability.

The 3D finite element analyses of gas storage caverns in domal salt deposits were performed by Hoffman (1993) to investigate the effects of cavern spacing on surface subsidence, storage loss, and cavern stability. In the paper by Staudtmeister et al. (1997), an optimal geometry for gas caverns in a domal deposit was proposed, considering hexagonal cavern fields with cylindrically shaped caverns and pillar width. Bruno (2005) analysed the influence of the distance between two caverns on cavern stability and deformation, considering distances equivalent to 2 and 3 cavern diameters. In the study conducted by Sobolik and Ehgartner (2006), a numerical analysis was carried out for a cavern field consisting of 19 cylindrical-shaped oil storage caverns in a salt dome. The results focused on the safety factor of salt pillars based on the dilatancy criterion. Another study by Park and Ehgartner (2011) investigated existing oil storage caverns in three salt domes. In this study, the minimal pillar width to cavern diameter ratio (P/D) was determined for each salt dome based on the rock salt dilatancy criterion. The P/D ranged from 0.52 to 0.92. The safety factor required for pillar or cavern stability is typically set at 1 (DeVries et al., 2005; DeVries, 2006; Van Sambeek et al., 1993). However, the safety factor for the minimal P/D determined in the cited study (Park et al., 2011) was found to be lower than 1. Nevertheless, the authors confirmed that all the analysed caverns were in a stable condition based on field observations. The cusp catastrophe model was employed by Wang et al. (2011) to evaluate the stability of pillars between two gas storage caverns in bedded salt deposits. The authors claimed that the cusp catastrophe model is more precise and practical compared to other models such as the finite element method (FEM). Wang et al. (2015a) investigated the allowable pillar width between two gas storage caverns using 3D numerical modelling. The results suggested that the width of the pillar should be 2.0–2.5 times (2D-2.5D) the cavern diameter. Another paper by Wang et al. (2015b) focused on the stability of two adjacent caverns near a fault in the Jintan salt mine. The minimum width of the pillar was determined to be at least two times (2D) the maximum cavern diameter. The location of a new cavern at a safe distance from the old cavern was investigated by numerical modelling in the paper by Wang et al. (2016). The results indicated that a safe pillar width is 2D. Yang et al. (2016) proposed a closely spaced cavern design for gas underground storage, analysing two groups composed of four caverns with a pillar width between adjacent caverns of 0.7D. The pillar between these two groups was set at 1.5D. Numerical simulations demonstrated that the stability of closely spaced caverns is possible under specific operating conditions.

In the paper by Zhang et al. (2017), a P/D ratio of 1.5 for oil storage caverns was found to be satisfactory for ensuring safety and resource management. In another paper by Yu et al. (2022), the safe pillar width for salt storage caverns was determined as larger than 1.2D for shallow rock salt layers (depth of 300–400 m). However, the same P/D ratio of 1.5 was unsatisfactory for gas storage caverns (Zhang et al., 2021). The theories related to the pillar design and stability were summarized by Ma et al. (2022). The authors highlighted that predicting salt cavern stability remains a complex problem that requires further research, as noted by Yu et al. (2022).

The previous research findings primarily focused on determining the optimal pillar width to ensure stability and efficient utilization of salt deposits. They also aimed to identify the failure mechanisms of pillars and establish the allowable pressure difference between adjacent caverns. These studies highlighted the complex nature of evaluating pillar stability, which is influenced by various factors. The objective of this paper is to investigate the influence of pillars width on their stability in relation to the number of caverns in the cavern field. Moreover, an allowable pillar width with regard to the number of caverns in the cavern field was analysed. Three different variants of pillar width were considered, and three cavern fields, each comprising a different number of caverns, are considered in the analysis. Additionally, the study aims to investigate the distribution of stresses and deformations in a cavern field in relation to the pillar width and number of caverns. The geological conditions and material properties of the Mechelinki salt deposit in Northern Poland are utilized in the study.

2 Modelling approach and Assessment Criteria

2.1 Shape of cavern

The assessment of optimal pillar width was based on numerical modelling. The numerical simulations aimed to find the optimal pillar width in given geological conditions. The pillars between solution mined caverns are irregular in shape, and this makes geomechanical analysis difficult (Zhang et al., 2021). To avoid the influence of the cavern shape on the results of analysis, a shape of cavern was based on cylinder.

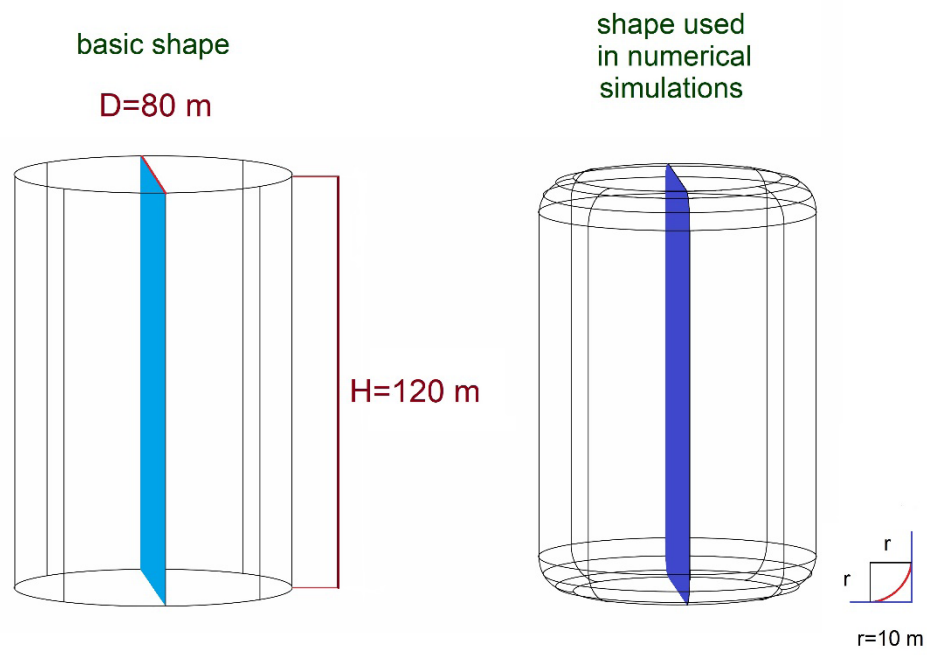

Figure 1: Shape and dimensions of caverns used in numerical simulations.

Previous study (Cyran & Kowalski, 2021) demonstrated that sharp edges in caverns lead to stress concentration and reduced stability. To address this issue, the cavern edges were smoothed by incorporating a quadrant with a radius of 10 m in the corners of a vertical cross-section of the cylindrical cavern shape (Fig. 1). Consequently, the original cylindrical shape of the cavern was transformed into a cylinder with slightly smoothed edges. This adjustment aimed to mitigate the stresses associated with sharp edges, which have an impact on pillar stability. The dimensions of examined caverns were tailored to the geological conditions of the Mechelinki salt deposit. The analysed shape is based on the assumed cavern height (H) of 120.0 m and a maximum diameter (D) of 80.0 m (Fig. 1). The thickness of the roof pillar was set to 15 m, while the bottom pillar had a thickness of 5 m.

2.2 Layout of the cavern field

To precisely asses the pillar width in a cavern filed, all the caverns in the filed should be modelled. In the present paper, the layout of the cavern field was based on concentric rings to ensure an equal distance (pillar width) between adjacent caverns and optimize the utilization of the salt deposit. The cavern field consisted of three rings (circles) with varying numbers of caverns. In the numerical analysis, three variations of cavern layouts associated with circles, as shown in Fig. 2, were considered. The first variant of the cavern layout comprised seven caverns (one central and six surrounding caverns). In the second variant, the cavern layout encompassed circles 1 and 2, totalling 19 caverns, including 7 from circle 1 and 12 from circle 2. The third variant of the cavern layout incorporated three circles, resulting in a total of 37 caverns, including 7 from circle 1, 12 from circle 2, and 18 from circle 3. Additionally, three variants of pillar width were evaluated: 1D (80.0 m), 2D (160.0 m), and 3D (240.0 m), respectively. A 60º wedge section represents caverns from each circle, including the cavern in the centre.

2.3 Numerical model and mechanical parameters

The geomechanical model of the cavern field was built based on the geological structure of the Mechelinki salt deposit. The salt beds belong to the Zechstein salt formation (cyclothem PZ1) and are situated at a depth of 960–980 m below ground level (b.g.l.). The thickness of the salt layers ranged from 160 to 190 m. The salt beds are underlain and overlain by anhydrite layers: the lower anhydrite (A1d) and the upper anhydrite (A1g). The thicknesses of these anhydrite layers range from about 1.5 to 20.0 m. The salt beds are underlain by Kupferschiefer (T1), Zechstein Limestone (Ca1), and Rotliegend and

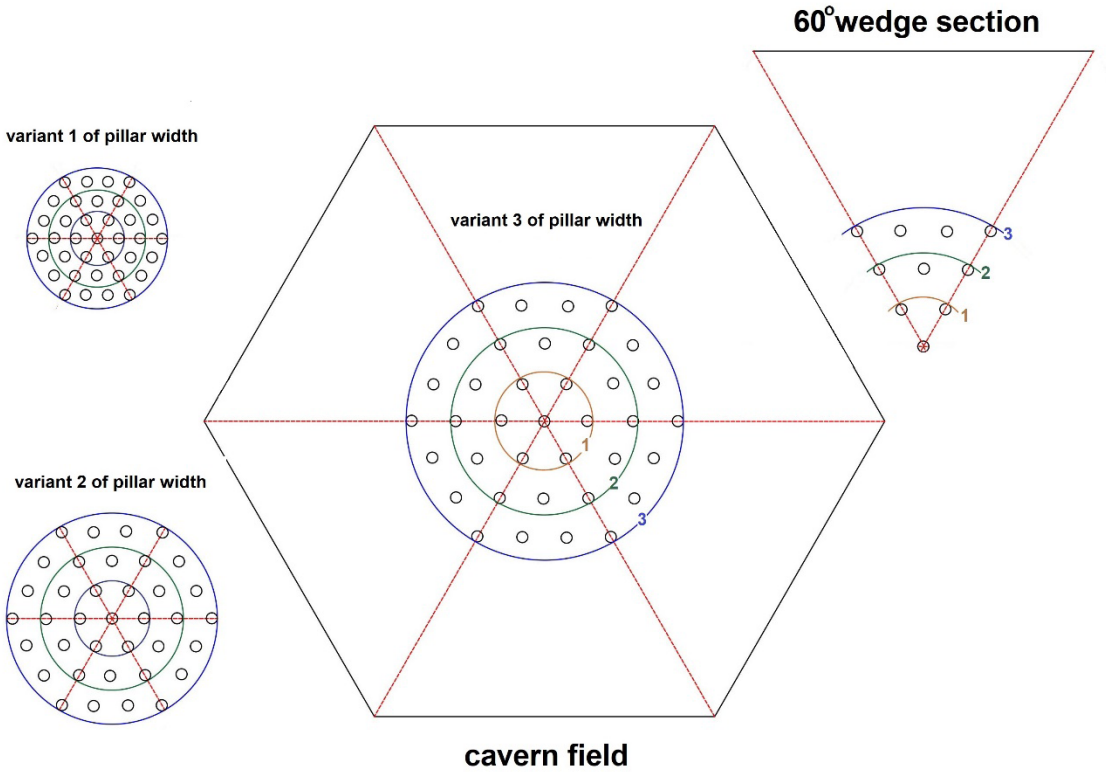

Figure 2: The layout of the cavern field:1, 2, 3 – ring number, pillar width in variant 1 – 80.0 m, variant 2 – 160.0 m, and variant 3 – 240.0 m.

Silurian sediments. The PZ2 and PZ3 sediments overlay the salt beds, along with Triassic, Jurassic, Cretaceous, and Cenozoic strata (Czapowski et al., 2007).

The numerical simulations were conducted for cavern fields consisting of 7, 19, and 37 individual caverns (Fig. 2). Boundary conditions were applied in the form fixed displacement in the normal direction on the side and bottom planes. The geometry of the model took the shape of a wedge (Fig. 2) with the base being an equilateral triangle, with sides measuring 2500 m and a height of 1500 m. The direct roof and the bottom of the rock salt beds consisted of anhydrite layers with a thickness of 30 m at the roof and 20 m at the bottom. Above and below the anhydrite layers, rock mass was located (Fig. 3). The upper layer with a thickness of 60 m was made up of soils. The roof of the rock salt beds was located at 975 m b.g.l. (Fig. 3). The mesh consisted of approximately 3.8 million elements, predominantly hexahedral. To enhance the efficiency of numerical simulations and ensure an accurate representation of the pillar width, the element size at the sidewalls of the pillars was smaller than that of the others (approximately 4 m). Outside the pillars, the sidewall elements were larger (around 50 m). The initial value of the hydrostatic stress varied with depth, ranging from 0 MPa at the top to 36.00 MPa at the bottom of the 3D model.

The rock mass mechanical behaviour was simulated with the use of the mechanical parameters and the constitutive models of the rock salt and the nonsalt rocks. Two different constitutive models were chosen to accurately project the viscoelastic plastic behaviour of rock salt and the elastic–plastic response of nonsalt rocks. The two-component Norton Power Law with a Mohr–Coulomb plasticity criterion was applied to describe the plastic yielding and creep of rock salt. However, the Mohr–Coulomb elastic–plastic model was used to simulate the mechanical behaviour of the surrounding rocks and the anhydrite.

The mechanical parameters of rock salt and nonsalt rocks were determined based on laboratory tests and validated in previous studies (Cała et al., 2018; Cyran et al., 2021). The parameters presented in Table 1 describe four materials: rock salt, anhydrite, rock mass, and soil. These mechanical parameters were applied to the numerical calculations. In addition, creep parameters for rock salt were determined in laboratory tests and calculated based on the Norton Power law. The creep parameters for rock

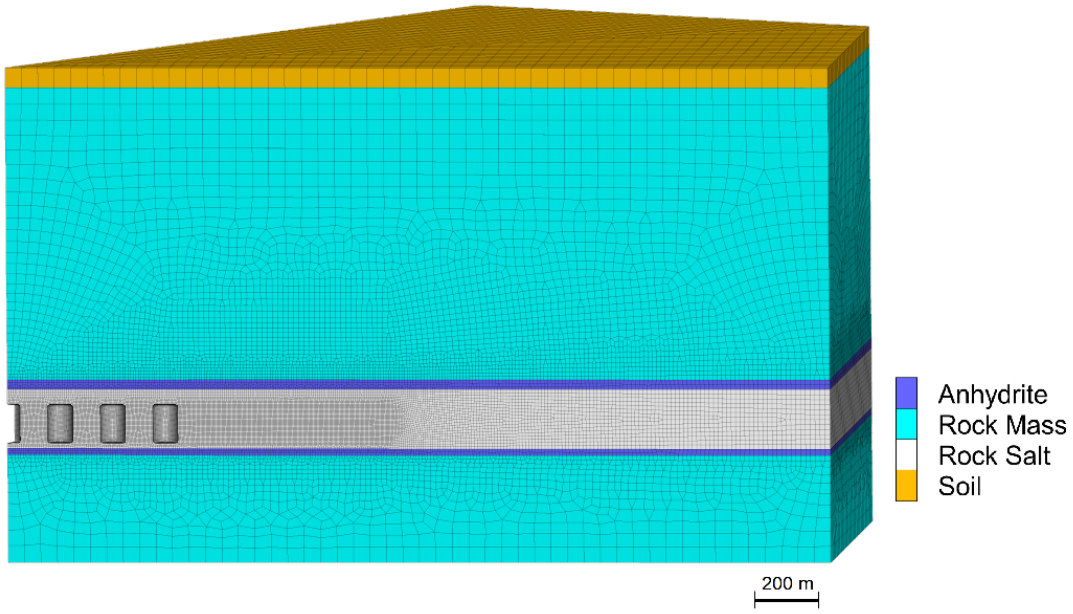

Figure 3: The numerical model of the cavern field based on the geological structure of the Mechelinki salt deposit.

Table 1: Mechanical parameters applied in the geomechanical analysis.

Parameters	Anhydrite	Rock Salt	Rock Mass	Soil
Bulk density (kg/m3)	2,400	2,400	2,400	2,000
Young's modulus (MPa)	12,000	5,000	10,000	100
Poisson's ratio (-)	0.20	0.45	0.25	0.25
Cohesion (kPa)	4,000	10,990	5,000	1
Internal friction angle (◦)	35	36.4	40	25
Tensile strength (kPa)	1,000	2,000	2,000	1

salt used in the numerical simulations are n = 5.0 and A = $1.08{\cdot}10^{-45}$ $Pa^{-5.0}$ s^{-1}.

2.4 Method of Analysis and Assessment Criteria

The evaluation of the pillar width was based on numerical modelling. The 3D geomechanical model of the cavern field was introduced into FLAC3D software, which is a tool for solving geomechanical and geotechnical problems, including rheological phenomena.

The relationship between pillar width and stability was assessed with the use of the following criteria (stability factors): deformations including the total displacements, vertical and horizontal displacements, von Mises stress (vMS), strength/stress ratio (SSR), and safety factor (SF). The total displacements were analysed at the sidewalls of the pillars because they reflected the changes in the pillar shape and volume caused by the salt creep. The vertical displacements show an overburden impact on the pillar. The horizontal displacements show the influence of the volume changes in salt caverns on the pillar, causing the pillar to shrink or expand. The vMS is the equivalent effective stress that is related to the creep rate within the primary and secondary creep stages. The von Mises stress (vMS) is expressed by equation *(1)*:

$$\sigma_{vm} = \sqrt{\frac{[(\sigma_1-\sigma_2)^2 + (\sigma_2-\sigma_3)^2 + (\sigma_3-\sigma_1)^2]}{2}} \quad (1)$$

where σ_{vm} is a von Mises stress, σ_1 is a major principal effective stress, σ_2 is an intermediate principal effective

stress, and σ_3 is a minor principal effective stress. The vMs indicates zones of large stress concentration which are important due to difference in mechanical behaviour between rock salt and other rocks such as anhydrite overlying and underlying rock salt. Rock salt exhibits rheological behaviour, but in the case of anhydrite, rheology can be ignored.

The strength/stress ratio (SSR) is used to indicate the dangerous areas in the pillars and surroundings. The strength–stress ratio (SSR) is a local indicator of a current stress state and its proximity to failure. SSR is described by equation *(2)*:

$$SSR = \left|\frac{\sigma_1' - \sigma_3}{\sigma_1 - \sigma_3}\right| \leq 10 \quad (2)$$

where σ_1' is the minimum effective principle stress in the failure state, σ_1 is the current minimum effective principle stress, and σ_3 is the current maximum effective principle stress.

An SSR equal to 1.0 implies a material failure, and furthermore, an SSR of 2 indicates that the material reaches 50% of its strength.

The safety factor (SF) is based on a dilatancy damage criterion for rock salt that can be expressed by equation *(3)*:

$$SF = \frac{b \cdot I_1}{\sqrt{I_2}} \quad (3)$$

where b is a material constant, I_1 is the first invariant of the stress tensor, and I_2 is the second invariant of the deviatoric stress tensor. When SF < 1, the shear stresses in the salt (J_2) are large relative to the mean stress (I_1), and dilatant behaviour is predicted. SF indicates material damage when it is below 1.0 (DeVries et al., 2005; DeVries, 2006; Sobolik et al., 2006; Sobolik & Ehgartner, 2006; Van Sambeek et al., 1993). This damage threshold indicates the onset of damage. It is important to note that a very short-term occurrence of a SF less than 1.0 does not necessarily result in immediate salt fracturing. The greater concern would be a value less than 1.0 over a period of several weeks or months, indicating that the accumulation of damage would cause fracture generation (Sobolik, 2016).

In addition, the changes in the pillar volume reflected by the cavern volume shrinkage (convergence) were evaluated. The cavern volume shrinkage was calculated as the ratio of the volume loss to the initial cavern volume.

The numerical analysis was carried out for a period of 12 years. Water leaching was employed for excavating the salt caverns. Upon completion of excavation, brine filled the entire salt cavern for a duration of 2 years subjecting the internal surface of the salt cavern to hydraulic pressure. Subsequently, brine was discharged from the caverns by natural gas, initiating cavern operation. During operation, load conditions were simulated by changes in cavern pressure. Ten operation cycles were simulated with cavern pressure oscillating between a minimum of 4 MPa and a maximum of 17.5 MPa. For each operation cycle, the assessment criteria mentioned above were analysed for 4 operation periods: at the beginning of the gas injection period, at the end of the gas injection period, at the beginning of the gas withdrawal period, and at the end of the gas withdrawal period. The numerical simulations assumed simultaneous and instantaneous leaching of all caverns in the applied software. Consequently, the displacements during the leaching period were minimal compared to those during the operation period, and their role in long-term cavern stability could be neglected. To mitigate the adverse effect of this assumption on the results, in-situ stress redistribution was calculated initially and used as the initial conditions for subsequent calculations, including creep.

3 Results

The results of numerical simulations of the pillar width are presented in the form of maps (Figs. 4–12). These maps display the value and distribution of the analysed factors, including displacements, vMS, SSR, and SF, during the last cycle (the last gas withdrawal and injection). A colour scale is used to represent the values of each factor, as shown on the left side of each map. The figures in the text highlight the most significant changes in the value and distribution of the simulated factors. The validation criteria for these simulations were described in Chapter 2.4.

The maps present cross-sections through the 60º wedge section, which represents caverns from each ring (ring nos 1, 2, and 3). In the cross-section through ring no. 1, two caverns are shown. The cross-section through ring no. 2 includes three caverns (two from ring no. 1 and one from ring no. 2), and through ring no. 3 shows four caverns (two from ring no. 1, one from ring no. 2, and one from ring no. 3). The figures indicate the ring numbers, and each map includes numbered caverns to facilitate reading. Cavern no. 1 is located in the centre of the cavern field, while cavern no. 4 is located at the edge of the cavern field.

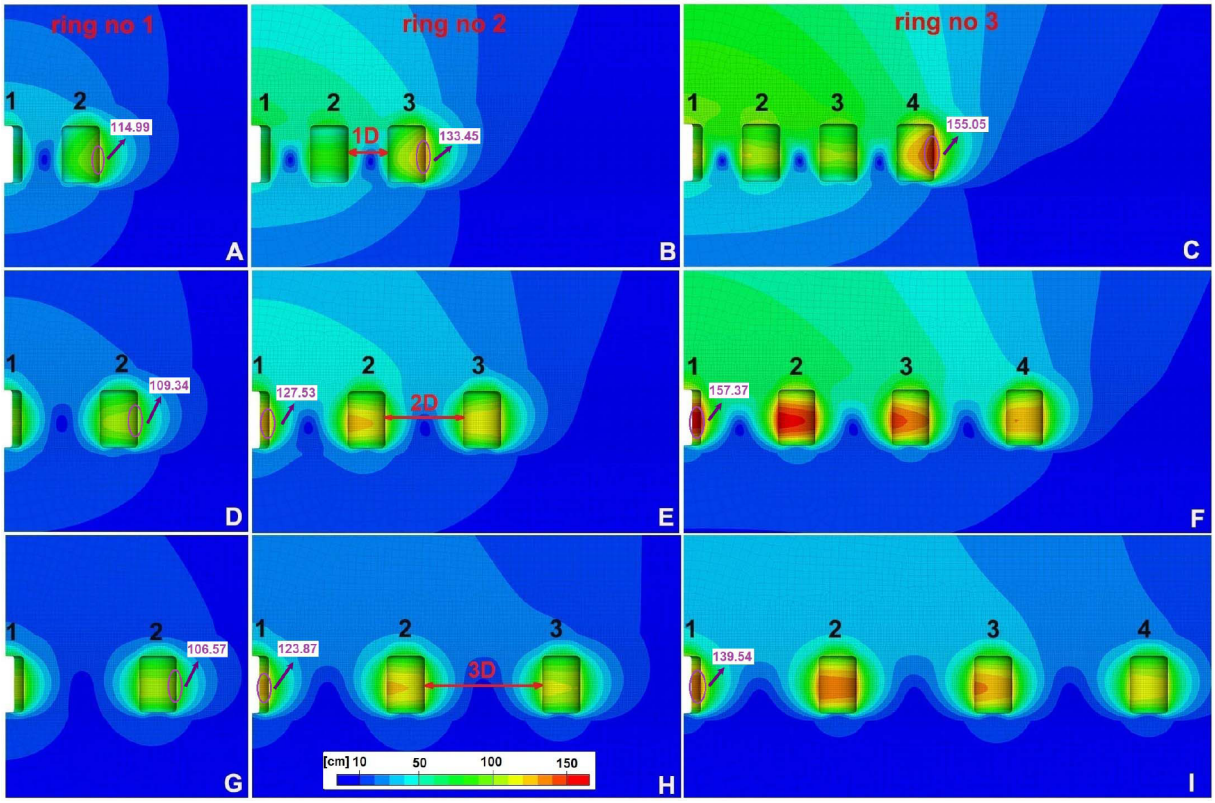

Figure 4: Total displacements in the pillars and the contour zone around the salt caverns for different pillar widths and cavern fields at the end of the last withdrawal period. The variants of cavern layouts are presented in rows, while the variants of pillar width are presented in columns. The largest values of total displacements were marked by the purple circle.

During each operation cycle, the largest displacements (total, vertical, and horizontal displacements) and vMS occurred at the end of the last withdrawal period for all analysed pillar widths (Figs. 4–8). The SSR and convergence were the lowest during the last withdrawal period (Fig. 10, 12), while the SF was the lowest at the beginning of the last gas withdrawal period (Fig. 11). Therefore, the maps depicting these periods are presented below.

3.1 Displacements

Displacements in the pillars between adjacent caverns are primarily caused by the creep behaviour of rock salt. The analysis focused on the total, vertical, and horizontal displacements of the rock mass within the pillars and surrounding the caverns. As a result of rock salt creep, the volume of the caverns decreases over time, leading to changes in the pillar width. These changes are visible in the displacements maps.

The distribution of total, vertical, and horizontal displacements during the last withdrawal period is presented in Figs. 4, 5, and 6, respectively. In the maps depicting vertical displacements, upward displacements are represented as positive values, while downward displacements are shown as negative values (Fig. 5 A–I). The vertical displacements demonstrate the influence of the overburden load on the pillars. Regarding horizontal displacements, both positive and negative values are observed (Fig. 6A–I). The sign of the displacement indicates its direction along the X axis. Positive horizontal displacements are directed outward from the centre of the cavern field, while negative horizontal displacements are directed inward toward the centre of the cavern field.

The maximum displacements, indicated in red, are predominantly located in the contour zone surrounding the caverns. These values gradually increase as the width of the pillar between two adjacent caverns decreases and the number of caverns in the ring increases (Fig. 4 A–I).

The results indicate that when only caverns in variant 1 of the cavern layout are analysed and the pillar width is 1D, 2D, or 3D, the maximum displacements are 114.99 cm, 109.34 cm, and 106.57 cm, respectively (Fig. 4A, D, G). However, when caverns in variant 3 of cavern layout are taken into account, the maximum displacements in the

pillar are 155.05 cm, 157.37 cm, and 139.50 cm, respectively (Fig. 4C, F, I). Increasing the distance between caverns leads to changes in the distribution and magnitude of displacements in the pillar between adjacent caverns and the area above the caverns. Notably, the contour zone around the caverns in variant 3 of cavern layout exhibits significant differences among the pillar widths of 1D, 2D, and 3D (Fig. 4C, F, I).

The maximum displacements of 139.5 cm and 157.37 cm are observed around caverns 1 and 2 (inner caverns) with a pillar width of 3D and 2D (Fig. 4F, I), respectively. However, for a pillar width of 1D, the maximum displacements are only found around cavern 4 (outer cavern) (Fig. 4C). It should be noted that increasing the pillar width to 2D results in an increase in the maximum displacement values for caverns in ring nos 2 and 3. However, for a pillar width of 1D, large displacements ranging from 90.0 to 100.0 cm are observed in a larger area (shown in green) (Fig. 4C). This area includes the upper part of the pillars between caverns 1, 2, and 3, as well as a significant zone above these caverns. Increasing the pillar width to 2D has a positive impact, as the displacements in the upper part of the pillars and above the caverns decrease to 60.0–70.0 cm between caverns 1 and 2 and 50.0–60.0 cm between caverns 2 and 3. Further increasing the pillar width to 3D results in additional decreases in displacements to 30.0–40.0 cm (shown in blue) in the upper part of the pillars and above the caverns.

Increasing the number of caverns in the ring affects the total displacements and their distribution. The large displacements, reaching 80.0–90.0 cm (Fig. 4B) between adjacent caverns 1 and 2, are observed in the upper part of the pillars with a width of 1D in ring no. 2. These displacements increase to 100.0–110.0 cm in ring no. 3 (Fig. 4C). Similar trends are observed for a pillar width of 2D. The displacements in the upper part of the pillars between adjacent caverns 1 and 2 range from 40.0 to 50.0 cm in ring no. 2 (Fig. 4E) and increase to 60.0–70.0 cm in ring no. 3 (Fig. 4F).

Vertical displacements in the pillar decrease as the pillar width increases. However, an increase in the number of caverns in the ring leads to higher values and extensions of vertical displacements. The largest downward displacements are mainly located above the cavern roof (blue) and below the bottom (orange), transferring to the pillars (Fig. 5A–I). The vertical displacements in the upper parts of the pillars and caverns are predominantly downward, while those in the lower parts are mainly upward. On average, the vertical displacements of the pillars are small, but locally they can be larger. For a pillar width of 1D, vertical displacements range from -70 cm to -90 cm in the upper part of the pillars and from 30 cm to 50 cm in the lower part (Fig. 5B, C). The load is mainly applied to the inner caverns (1 and 2) in ring nos 2 and 3. Increasing the pillar width to 2D decreases the magnitude and extension of vertical displacements (Fig. 5D–F), but the area of downward displacements (-50 cm to -60 cm) in the upper part of the pillar between the inner caverns (1 and 2) remains. Enlarging the pillar width to 3D further reduces this area.

The horizontal displacements in the caverns and pillars contribute to the shrinkage of cavern volume and the tension in the pillars (Fig. 6A–I). The distribution of horizontal displacements shows that they are the largest in the contour zones around the caverns and gradually decrease towards the centre of the pillar. However, this zone is wide when the pillar width is 1D and extends over most of the pillar (Fig. 6A–I). For a pillar width of 1D, there is a significant difference between the values of positive and negative horizontal displacements. This difference decreases as the pillar width increases and reaches almost the same value for a pillar width of 3D. In the cross-section through ring no. 1, the maximum values of horizontal displacements are -114.92 cm and 63.35 cm for a pillar width of 1D (Fig. 6A), whereas they are -106.38 cm and 103.90 cm for a pillar width of 3D (Fig. 6C). This large difference in horizontal displacements for a pillar width of 1D causes unevenly distributed tension in the pillars. The largest horizontal displacements, directed inside the centre of the cavern field, are distributed in the contour zone of all caverns when the pillar width is 2D and 3D (Fig. 6D–I), but they are distributed in the contour zone of the outer caverns when the pillar width is 1D (Fig. 6A–C). An increase in the number of caverns in the field leads to an increase in both positive and negative horizontal displacement values for all analysed pillar widths (Fig. 6A–I). Interestingly, there is an increase in the value of horizontal displacements for a pillar width of 2D in both rings 2 and 3 (Fig. 6E, F) compared to a pillar width of 1D and 3D.

The results indicate that the total and horizontal displacements in the pillars are largest in the contour zone around the caverns and gradually decrease towards the centre of the pillar (Figs. 4, 6). The vertical displacements are largest in the upper and lower parts of the pillars (Fig. 5). The value and range of total and vertical displacements decrease with an increase in the pillar width (Figs. 4–5), but the value of horizontal displacements increases with the pillar width (Fig. 6). In general, the values of total, vertical, and horizontal displacements increase when the number of caverns increases (Figs. 4–6). The largest vertical displacements are associated with the pillars

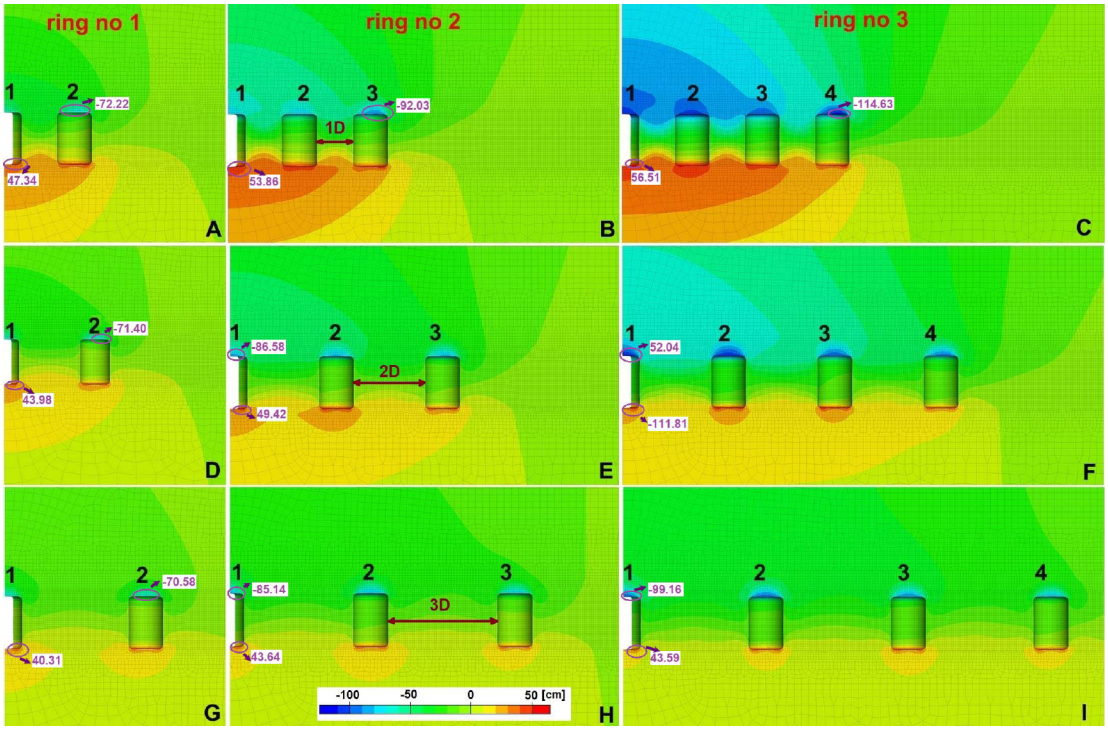

Figure 5: Vertical displacements in the pillars and the contour zone around the salt caverns for different pillar widths and cavern fields at the end of the last withdrawal period. The variants of cavern layouts are presented in rows, while the variants of pillar width are presented in columns. The largest values of vertical displacements were marked by the purple circle.

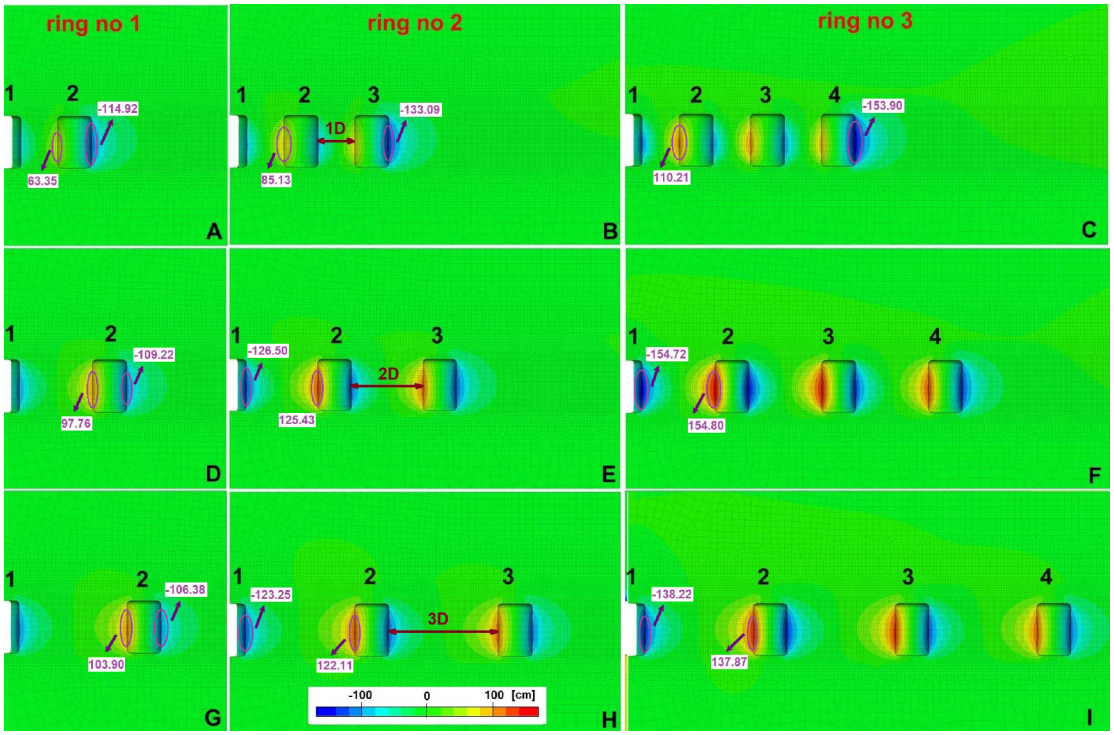

Figure 6: Horizontal displacements in the pillars and the contour zone around the salt caverns for different pillar widths and cavern fields at the end of the last withdrawal period. The variants of cavern layouts are presented in rows, while the variants of pillar width are presented in columns. The largest values of horizontal displacements were marked by the purple circle.

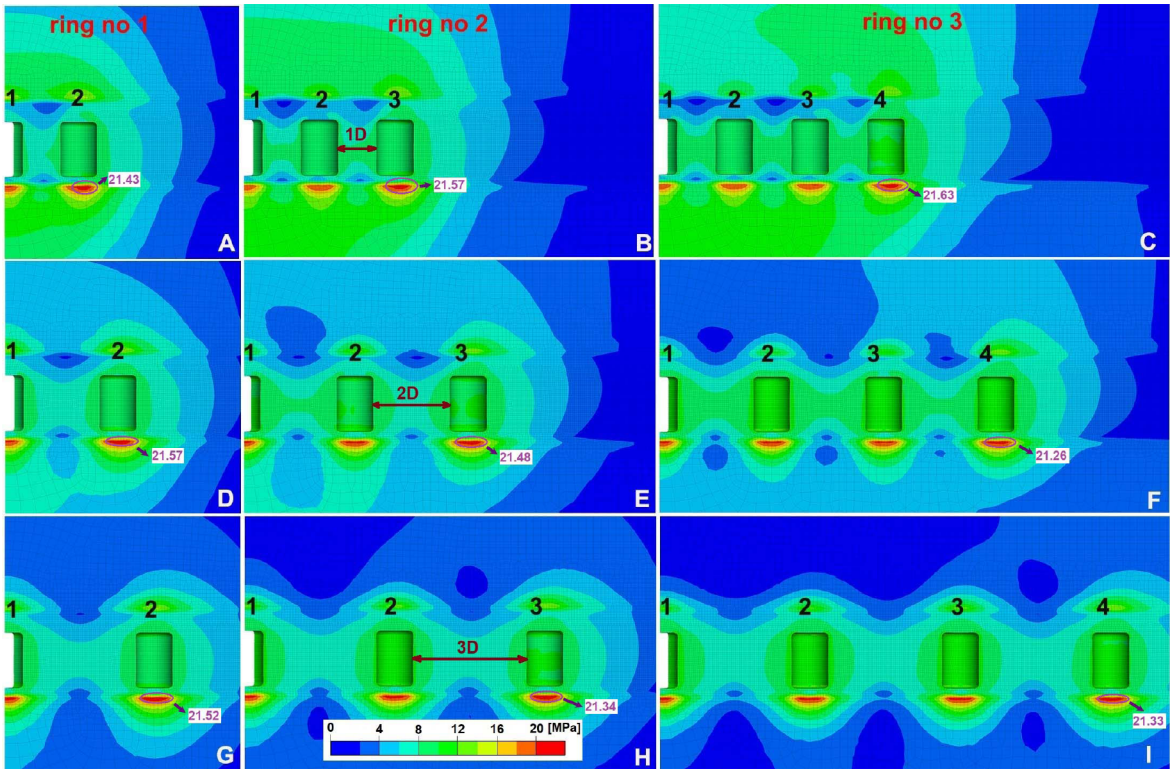

Figure 7: Von Mises stress in the pillars and contour zone around the salt caverns for different pillar widths and cavern fields at the end of the last withdrawal period. The variants of cavern layouts are presented in rows, while the variants of pillar width are presented in columns. The largest values of von Mises stress were marked by purple circle.

between adjacent caverns located in the inner part of the cavern field (Fig. 5). The largest total displacements are found in the inner part of the cavern field consisting of 19 or 37 caverns when the pillar width is 2D and 3D (Fig. 4E, F, H, I). However, when the cavern field consists of only 7 caverns, the largest total displacements occur at the edge of the cavern field (Fig. 4D, G). Similarly, when the pillar width is 1D, the largest total and horizontal displacements are located at the edge of the cavern field (Fig. 4 B, C). The increase in the value of total and horizontal displacements for ring nos 2 and 3, and a pillar width of 2D, indicates that this pillar width is insufficient to provide stability. Therefore, the allowable pillar width for a cavern field consisting of 19 and 37 caverns should be between 2D and 3D.

3.2 Von Mises stress

The maps in Figure 7A–I present the values and distribution of von Mises stress (vMS) during the last withdrawal period. The maximum vMS value (red colour) is associated with the area below the cavern bottom and ranges from 21.63 to 21.13 MPa. The extent of these areas remains the same regardless of the pillar width and number of caverns. The range of vMS values between 14.0 and 16.0 MPa is located in the area above the roof of the cavern. The extent of these areas is more influenced by the number of caverns rather than the pillar width.

The overall vMS values in the pillars are relatively low, mostly ranging between 8.0 and 10.0 MPa (Fig. 7 A–I). However, in certain areas of the pillars, the vMS ranges from 10.0 to 12.0 MPa when considering ring nos 2 and 3 (Fig. 7 B, C, E, F, H, I). Additionally, as the pillar width increases, the vMS decreases. For example, in variant 3 of cavern layout, the vMS reaches 8.0–10.0 MPa and 6.0–8.0 MPa when the pillar width is 2D and 3D, respectively.

The results in Figure 8 show that areas of the pillars with slightly higher vMS values (10.0–12.0 MPa) are associated with the contours surrounding the caverns. The distribution of these areas varies for different pillar widths and the number of caverns in the ring. When the pillar width is 1D, the vMS of 10.0–12.0 MPa is associated with the contours surrounding the outer caverns (Fig. 7 A–C). The same distribution of vMS values is observed for in variant 1 of cavern layout and pillar widths 2D and 3D (Fig. 7 D, G). However, for pillar widths 2D and 3D and ring nos 2 and 3 (Fig. 7 E, F, H, I), this value (10.0–12.0 MPa)

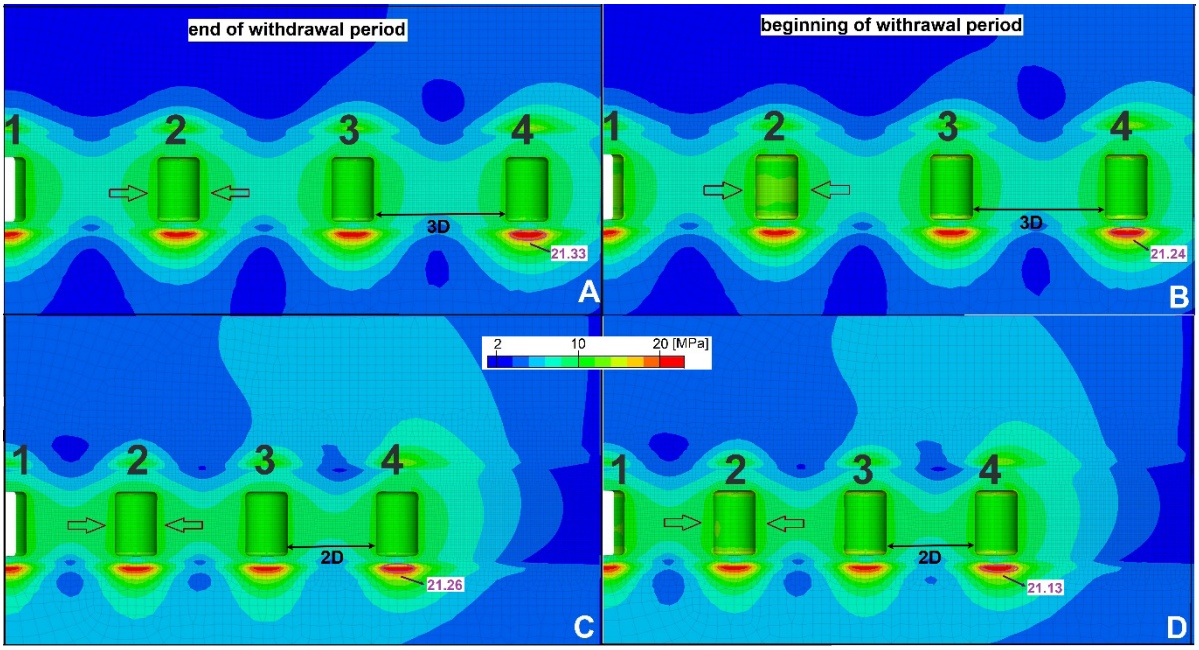

Figure 8: Von Mises stress in the pillars and contour zone around the salt caverns for different pillar widths at the end and beginning of the last withdrawal period, a cross-section through ring no. 3. The largest values of von Mises stress were marked by the purple circle.

of vMS is found in the contours surrounding all caverns. Moreover, the results show an increasing proportion of areas where the vMS value is 6.0–8.0 MPa with an increase in the pillar width.

It is worth noting that there is a difference in vMS between the beginning and end of the last withdrawal period. Although the maximum vMS value is slightly higher (21.33–21.63 MPa) at the end of the withdrawal period compared to the beginning (21.13–21.33 MPa), the distribution of vMS values differs between these two periods (Figs. 7, 8). The vMS ranges from 10.0 to 12.0 MPa in the contour zone around the caverns (Fig. 8A–D). This zone is larger at the beginning of the withdrawal period (Fig. 8B, D) and occurs around all caverns in cross-sections through ring nos 2 and 3. Furthermore, the vMS values of 8.0–10.0 MPa in the contour zone around all caverns are larger and occupy a larger area of the pillars at the beginning of the withdrawal period compared to the end (Fig. 8A–D).

The above results indicate that the vMS values in the pillars are generally low compared to the area below the cavern bottom (Figs. 7, 8). The largest value of vMS (10.0–12.0 MPa) in the pillars is related to the contour zone around the caverns and gradually decreases to the centre of the pillar where their value is the lowest (6.0–8.0 MPa). The overall vMS magnitude decrease when pillar width increases and increase with the number of caverns (Fig. 7A–I). Based on the above results, the pillar width 2D is safe for the long-term stability of the cavern field consisting of 7, 19, and 37 caverns (Figs. 7, 8).

3.3 Strength/stress ratio (SSR)

During the analysed time period of 12.5 years, there were variations in the strength/stress ratio (SSR) in the pillars between adjacent caverns. The lowest SSR values (1.73–1.87, dark blue colour) were observed in the area below the caverns (Fig. 10A–I). The extent of these areas is primarily influenced by the pillar width and decreases as the pillar width increases. Additionally, the SSR ranges from 3 to 3.5 over the roof of the cavern when the pillar width is 1D (Fig. 10 A–C) and 3.5–4.0 when the pillar width is 2D and 3D (Fig. 9 D–I). These SSR values and their distribution do not significantly affect the overall stability of the caverns.

In general, the SSR in the pillars between caverns is high, with most areas having values above 8.0 (Fig. 9A–I). In the contour zone around the caverns, the SSR value decreases to 4.5–5.5 when the pillar width is 2D and 3D (Fig. 9 D–I). When the pillar width is 1D, the SSR value of 7.0–8.0 covers most of the pillar area (Fig. 9 A–C).

The results presented in this section indicate that the SSR in the pillar is generally high compared to the area below the caverns (Fig. 9A–I). The SSR value is primarily influenced by the pillar width, where a larger pillar width corresponds to a higher SSR value. The lowest SSR values

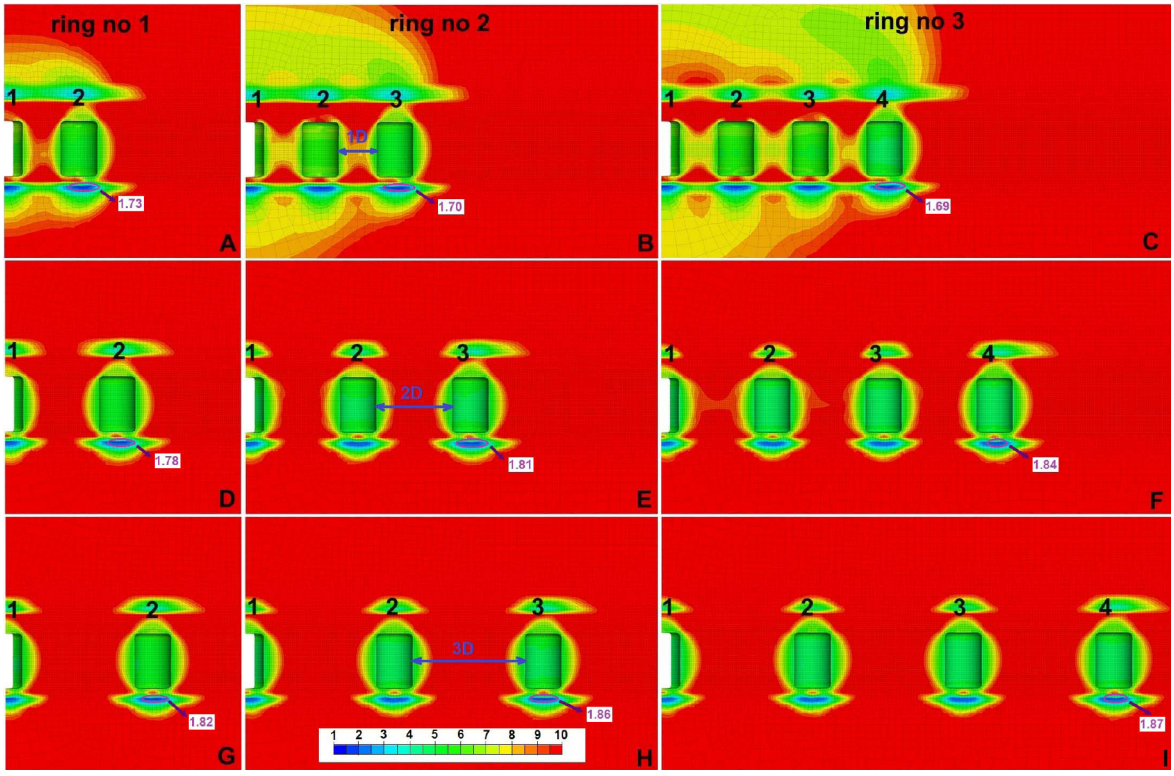

Figure 9: SSR in the pillars and the contour zone around the salt caverns for different pillar widths and cavern fields at the end of the last withdrawal period. The variants of cavern layouts are presented in rows, while the variants of pillar width are presented in columns. The lowest values of SSR were marked by the purple circle.

(4.5–5.5) in the pillars are associated with the contour zone around the caverns, and the SSR gradually increases towards the centre of the pillar (Fig. 9A–I). Based on these results, the SSR in the pillar, considering all analysed pillar widths and the number of caverns, is sufficiently high to ensure cavern stability. However, for overall cavern stability, including the area above the roof and below the bottom, the minimum allowable pillar width is 2D for all analysed cavern fields.

3.4 Safety factor (SF)

The SF (safety factor) value and its distribution exhibit variations for the analysed pillar width and number of caverns in the cross-section. The lowest SF values range from 3.09 to 3.32 and are locally indicated in the contour zone around the caverns (Fig. 10A–I). These SF values satisfy safety requirements for cavern stability, indicating no risk of dilatancy damage in the pillars during the analysed time period of 12.5 years.

Overall, the SF in the pillars is high, with most values exceeding 5.0 and some falling below 4.0 (Fig. 10A–I). In the contour zone around the caverns, the SF reaches 3.5–4.5 and gradually increases towards the centre of the pillar, where its value is the highest (Fig. 10A–I). These SF values are observed in areas above the roof and below the bottom of the caverns for all analysed variants. Some changes in the SF value and distribution are mainly influenced by the pillar width. For a pillar width of 1D, most areas of the pillar exhibit SF values above 5.0–6.0 (Fig. 10G–I). However, when the pillar width is 2D and 3D, the SF of 5.0–6.0 occurs only in the contour zone around the caverns (Fig. 10D–I). The distribution of the lowest SF is affected by both the pillar width and the number of caverns in the cross-section. When the pillar width is 1D, the lowest SF values (3.09–3.32) occur in individual elements (Fig. 10A–C). The lowest SF values of 3.17–3.28 are locally indicated around the middle part of the caverns for a pillar width of 2D and 3D in ring nos 2 and 3 (Fig. 11D–I).

Based on the above results, it is evident that the overall SF in the pillar is sufficiently high to meet safety requirements. The value and distribution of SF are primarily influenced by the pillar width (Fig. 10A–I). The SF in the pillars increases with the pillar width. The lowest SF values (3.0–3.5) in the pillars are associated with the contour zone around the caverns and gradually increase towards the centre of the pillar (Fig. 10A–I).

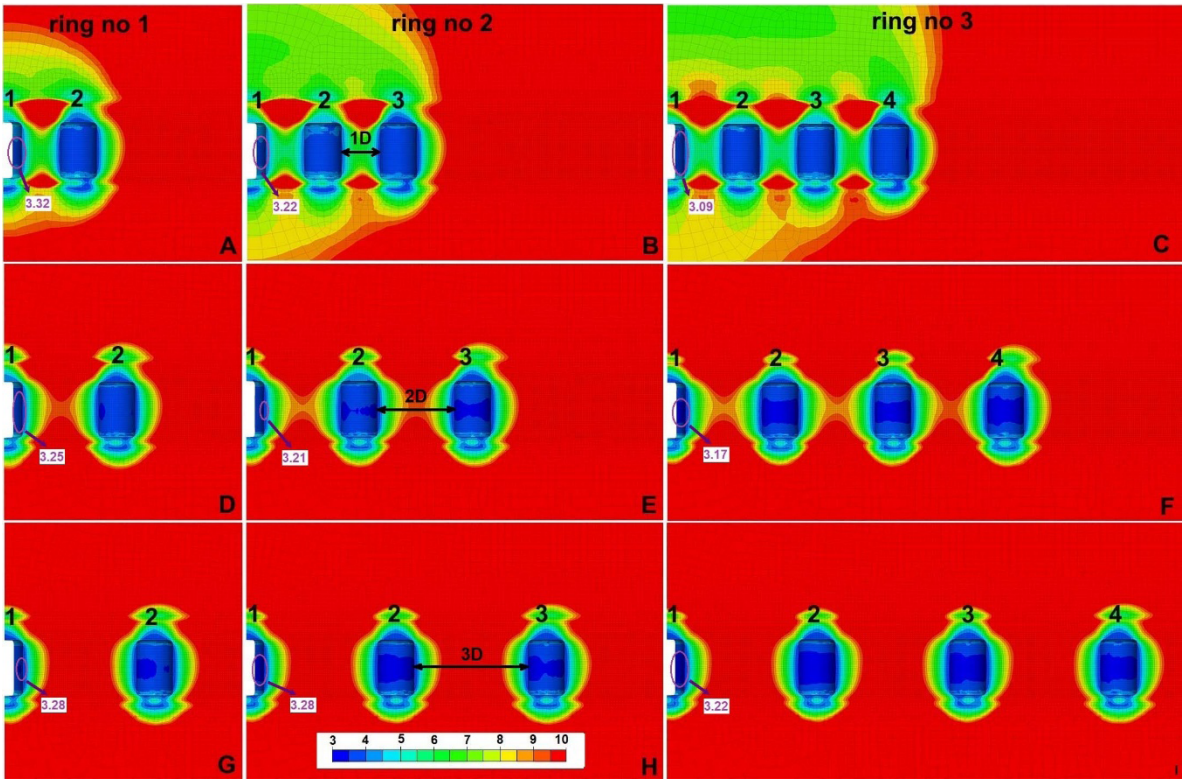

Figure 10: SF in the pillars and the contour zone around the salt caverns for different pillar widths and cavern fields at the beginning of the last withdrawal period. The variants of cavern layouts are presented in rows, while the variants of pillar width are presented in columns. The lowers values of SF were marked by the purple circle.

3.5 Volume shrinkage (convergence)

The results presented in Figure 11 demonstrate the changes in the cavern volume caused by injection and withdrawal cycles, resulting in volumetric shrinkage or convergence. The convergence is significantly higher during the withdrawal cycle compared to that during the injection cycle. These changes in the cavern volume also affect the pillar volume. Figure 11 illustrates that the impact of pillar width on convergence increases with the number of caverns. The influence of pillar width on convergence is relatively low for ring no. 1 (Fig. 11A) due to lower convergence values ranging from 4.5% (1D) to 5.3% (2D and 3D). For a cavern field consisting of 19 caverns (Fig. 11B, ring no. 2), the convergence ranges from 4.9% (1D) to 6.0% (2D). The largest influence of pillar width on volumetric shrinkage is observed for pillar ring no. 3 (Fig. 11C, 37 caverns), with convergence values of 5.6%, 6.2%, and 6.8% for pillar widths of 1D, 2D, and 3D, respectively. The highest volume shrinkage (6.80%) is estimated for a pillar width of 2D and a cavern field consisting of 37 caverns (ring no. 3). Similarly, for ring no. 2 (19 caverns), the pillar width 2D (Fig. 11B) showed the largest convergence (6.0%). The convergence is the lowest for pillar width 1D (Fig. 11A–C) and was estimated between 4.50% and 5.70%. These results align with the values and distribution of total and horizontal displacements (Figs. 4A–I, 6A–I).

4 Discussion

The analysis indicates that pillar stability improves with an increase in pillar width. Based on the results of the following stability criteria: displacements, vMS, SSR, SF, and volume shrinkage, the allowable pillar width should be greater than 2D. These findings are consistent with the conclusions drawn by Wang et al. (2015, 2016), Yang et al. (2016), Yu et al. (2022), and Zhang et al. (2021). When the pillar width is small, the applied load transfers to the rock mass surrounding the adjacent cavern, thereby increasing stresses and deformations (Wang et al., 2015). However, a reasonably set pillar width ensures that the influence of adjacent caverns decreases playing an insignificant role in stability (Zhang et al., 2021).

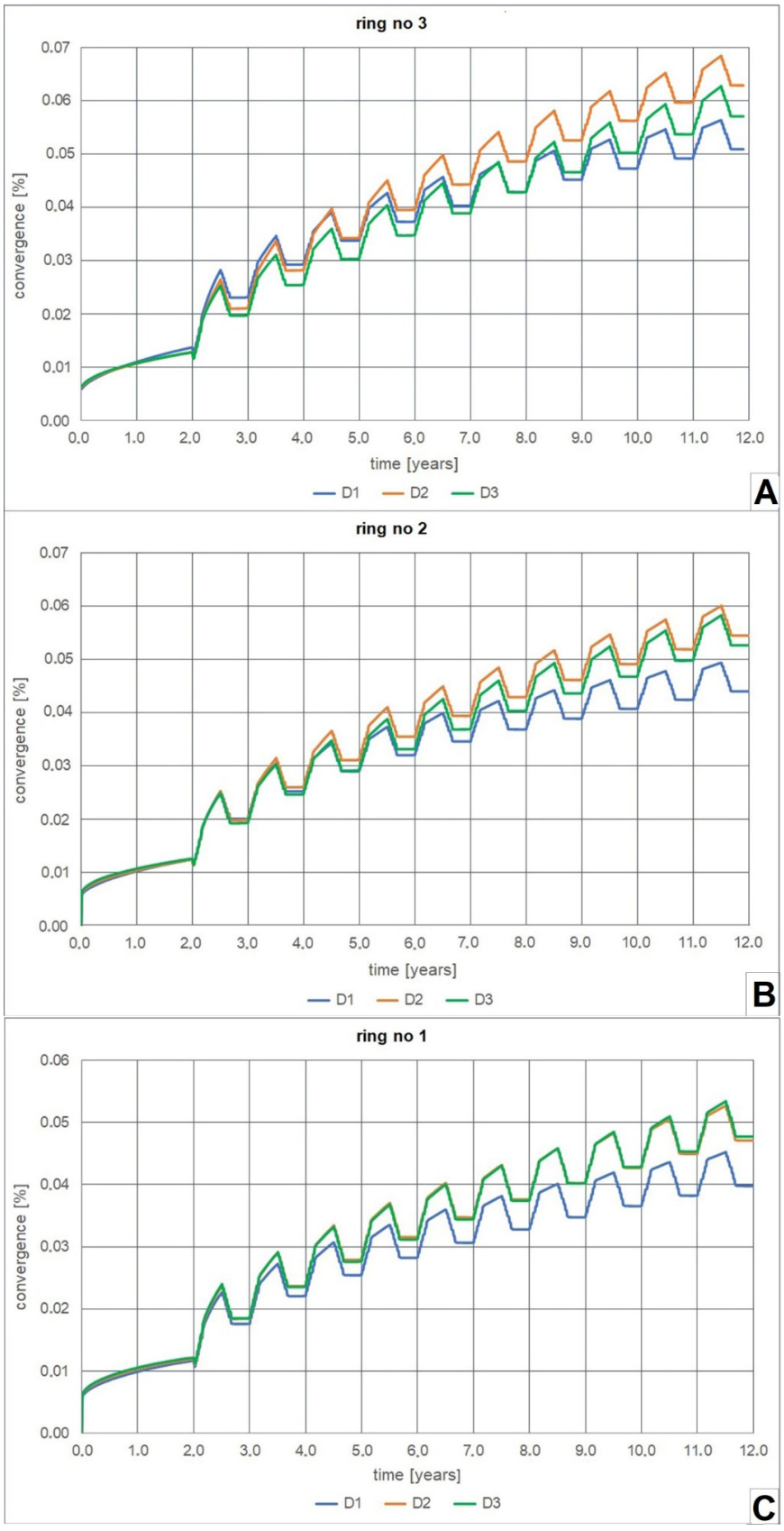

Figure 11: Convergence in the cavern fields for different pillar widths (D1, D2, D3) at the end of the last withdrawal.

The presented above results indicated that the values of all analysed stability criteria are unevenly distributed within the pillar. The pillars exhibit the poorest stability performance in the contour zone around the caverns, with better stability performance observed closer to the centre of the pillar. These differences are associated with the distribution of horizontal stress in the pillar and are reflected in the value and distribution of horizontal displacements.

The analysed variants of the pillar width show differences between the values of horizontal and vertical displacements, with horizontal displacements generally being larger than vertical displacements. It was found by Zhang et al. (2022) that when the horizontal stress exceeds the vertical pressure, the pillar undergoes tension, leading to damage. However, in performed simulations, the largest values of horizontal displacements occur in the contour zone around the caverns when the pillar width is 2D and 3D comprising only a narrow part of each pillar. These displacements are caused by the volume shrinkage of the caverns. Considering the maximal convergence after 12.5 years (6.80%), the risk of pillar damage is minimal. The authors in the paper by Yang et al. (2016) explained that when there is a significant difference in vertical displacement values between the lower and upper parts of the pillar caused by vertical pressure, local damage may occur. The results presented above indicate that the risk of local damage may occur only when the pillar width is 1D and is mainly related to the caverns located in the central part of the cavern field, which consists of 19 and 37 caverns.

Most authors such as Wang et al. (2011, 2015 a, b, 2016) and Zhang et al, (2017, 2020, 2021) have conducted numerical simulations of pillar width for two adjacent caverns. It was advised by Park et al. (2011) to evaluate pillar width only between pair of caverns because the thickness of the pillar between them varies as a function of depth and direction. However, the analysis performed in this study revealed that the number of caverns in the cavern field significantly influences pillar stability. The results of the numerical simulation indicated that for a cavern field consisting of 7 caverns (ring no. 1), a pillar width of 2D is sufficient to ensure stability. On the contrary, when the cavern field consists of 19 and 37 caverns (ring nos 2 and 3), the allowable pillar width should be greater than 2D due to large displacements in the upper part of the pillars and above the caverns located in the inner part of the field (cavern nos 1 and 2). These results suggest that numerical simulations performed only for two adjacent caverns give incomplete information about stresses and displacement distribution in the cavern field. These findings are especially important for planning cavern operation cycles because the uneven distribution of stresses and displacements between adjacent caverns may affect pillar stability. For instance, when the pressure in the two caverns is unequal, the pillar may undergo shear failure during the gas injection and production process (Ma et al., 2022).

An additional effect is related to the changes in pressure during injection and withdrawal cycles. The results presented above showed that the risk of dilatant failure is the largest at the beginning of the withdrawal cycle. It is caused by overburden load which is carried out by the pillar after caverns withdrawal (Wang et al., 2015). In the case of analysed pillars, SF was high and showed no risk of dilatant failure. However, the creep rate of rock salt is highest at the end of the withdrawal cycle because the pressure in caverns is maintained at a minimal level. Then, the vertical overburden stress exceeds the horizontal stress and may lead to damage caused by pillar expansion (Ma et al., 2022).

5 Conclusions

To ensure the safety of storage operation and rational use of rock salt resources, the effect of different pillar widths on the stability of cavern fields was evaluated in this study. A reasonable pillar width that provides the stability of the cavern field consisting of different numbers of caverns was analysed in numerical simulations. The conclusions drawn in this study were summarized as follows:

(1) The stability of pillars was evaluated using the following criteria: total, horizontal, and vertical displacements; vMS, SSR, and SF. The stability of pillars increases with an increase in pillar width. The applied load induces stresses and displacements in the rock salt mass surrounding the caverns. When the pillar width is too small, these stresses and displacements transfer into the pillars, adversely affecting their stability.

(2) The number of caverns in the cavern field has a significant effect on pillar stability. Based on the aforementioned stability criteria, when the cavern field consists of 19 and 37 caverns, the allowable pillar width between adjacent caverns should be between 2D and 3D. When the pillar width is 2D or less, the large horizontal displacements exert tension on the pillar, potentially causing damage. A pillar width of 3D ensures pillar stability but contradicts the rational use of rock salt resources. However, when the cavern field consists of 7 caverns, a pillar width of 2D is sufficient to meet the analysed stability criteria.

(3) The pillar stability performance is the best in the pillar centre and the worst in the contour zone around the caverns. The centre of the pillar is slightly affected by the pressure in the caverns resulting from withdrawal and injection cycles. However, the contour zone around the caverns (i.e., the edges of the pillar) experiences stress and deformation due to changes in the operating pressure of the caverns.

(4) The analysed stability criteria indicate that stresses and deformations are unevenly distributed within the cavern field. When the cavern field consists of 19 and 37 caverns and the pillar width is 2D and 3D, the pillars and caverns located inside the cavern field exhibit worse stability performance compared to those at the edge of the cavern field. This is attributed to the large total displacements observed in the pillars and above the caverns' roof located within the cavern field. However, when the pillar width is 1D, the largest total displacements are found at the edge of the cavern field. This uneven distribution of displacements results from the volume of the pillars, which is directly related to their width. With a pillar width of 1D, the smaller pillar volume and the bending of the caverns' roof due to the overburden load lead to horizontal stresses in the rock salt mass around the cavern field that are greater than the overburden stress. Consequently, the largest displacements are observed at the edge of the cavern field. When the pillar width is 2D and 3D, the larger pillar volume allows for the bearing of vertical and horizontal stresses. As a result, the bending of the caverns' roof and the horizontal stress led to the largest displacements occurring inside the cavern field.

(5) The findings presented in this study are valuable for the planning and design of cavern fields for underground storage of energy sources such as oil, natural gas, and hydrogen. These findings are particularly important for the planning of operation and production cycles in cavern fields since the uneven distribution of stresses and displacements between adjacent caverns affects pillar stability.

References

[1] Aubertin, J. D., Hoentzsch, S., Diederichs, M. S., & Milton, H. (2018). Influence of the Creep Law on Pillar Response Based on Numerical Simulations of an Underground Salt Mine. *52nd U.S. Rock Mechanics/Geomechanics Symposium, ARMA-2018-1331*.

[2] Baryakh, A. A., Lobanov, S. Yu., & Lomakin, I. S. (2015). Analysis of time-to-time variation of load on interchamber pillars in mines of the Upper Kama Potash Salt Deposit. *Journal of Mining Science*, 51(4), 696–706. doi: 10.1134/S1062739115040064

[3] Bruno, M. S. (2005). *Geomechanical Analysis and Design Considerations for Thin-Bedded Salt Caverns: Final Report*. CA, USA.

[4] Cała, M., Cyran, K., Kowalski, M., & Wilkosz, P. (2018). Influence of the Anhydrite Interbeds on a Stability of the Storage Caverns in the Mechelinki Salt Deposit (Northern Poland). *Archives of Mining Sciences*, *63*(4), 1007–1025.

[5] Cyran, K., & Kowalski, M. (2021). Shape Modelling and Volume Optimisation of Salt Caverns for Energy Storage. *Applied Sciences*, 11(1), 423. doi: 10.3390/app11010423

[6] Czapowski, G., Chełmiński, J., Tomaszczyk, M., & Tomassi-Morawiec, H. (2007). Metodyka modelowania przestrzennego budowy geologicznej osadowych złóż pokładowych na przykładzie cechsztyńskiego złoża soli kamiennej Mechelinki nad Zatoką Pucką. *Przegląd Geologiczny*, *55*(8), 681–689.

[7] DeVries, Kerry L, Mellegard, K. D., Callahan, G. D., & Goodman, W. M. (2005). *Cavern roof stability for natural gas storage in bedded salt*. Pittsburgh, PA, and Morgantown, WV (United States). doi: 10.2172/850074

[8] DeVries, K.L. (2006). Geomechanical analyses to determine the onset of dilation around natural gas storage caverns in bedded salt. *SMRI Spring Technical Meeting, Brussels*.

[9] Frayne, M. A., & Van Sambeek, L. L. (2001). Three-dimensional verification of salt pillar design equation. In Basic and Applied Salt Mechanics. London: CRC Press.

[10] Hoffman, E. L. (1993). *Effects of cavern spacing on the performance and stability of gas-filled storage caverns. Sandia Report SAND-92-2545*. Albuquerque, USA.

[11] Ma, H., Wei, X., Shi, X., Liang, X., Bai, W., & Ge, L. (2022). Evaluation Methods of Salt Pillar Stability of Salt Cavern Energy Storage. Energies 15, (20) 7570. doi: 10.3390/en15207570

[12] Park, Y. B., & Ehgartner, B. L. (2011). *Allowable Pillar to Diameter Ratio for Strategic Petroleum Reserve Caverns*. Sandia Report SAND2011-2896. Albuquerque, USA

[13] Qin, X. S., Cao, H., & Guo, L. J. (2020). Sensitivity analysis of factors influencing pillar stability in the deep stope of underground salt mine. *IOP Conference Series: Earth and Environmental Science*, 570(2), 022002. doi: 10.1088/1755-1315/570/2/022002

[14] Sobolik, S. R., & Ehgartner, B. L. (2006). *Analysis of Cavern Shapes for the Strategic Petroleum Reserve. SANDIA REPORT SAND2006-3002*. Albuquerque, USA.

[15] Sobolik, S.R., (2016). Assessment of the Available Drawdowns for Oil Storage Caverns at the West Hackberry SPR Site. Sandia Report SAND2016-3077. Albuquerque, USA.

[16] Staudtmeister, K., & Rokahr, R B. (1997). Rock mechanical design of storage caverns for natural gas in rock salt mass. *J. Rock Mech. & Min. Sci*, 34(4), 301-313. https://doi.org/10.1016/S1365-1609(97)00199-8

[17] Swift, G. M., & Reddish, D. J. (2005). *Underground excavations in rock salt*. Geotech Geol Eng 23, 17–42. https://doi.org/10.1007/s10706-003-3159-3

[18] Van Sambeek, Leo L., Ratigan, J. L., & Hansen, F. D. (1993). Dilatancy of rock salt in laboratory tests. *International Journal of Rock Mechanics and Mining Sciences & Geomechanics Abstracts*, 30(7), 735–738. doi: 10.1016/0148-9062(93)90015-6

[19] Van Sambeek, L.L. (1997). Salt Pillar Design Equation. In: Peng S. S. & Holland C. T. (Eds.), Proceedings of the 16th International Conference on Ground Control in Mining. Morgantown: West Virginia University.
[20] Wang, T., Yan, X. Z., Yang, H. L., & Yang, X. J. (2011). Stability analysis of the pillars between bedded salt cavern gas storages by cusp catastrophe model. *Science China Technological Sciences*, 54(6), 1615–1623. doi: 10.1007/s11431-011-4401-5
[21] Wang, T.; Yang, C.; Yan, X., & Daemen, J. J. K. (2015a). Allowable pillar width for bedded rock salt caverns gas storage. *Journal of Petroleum Science and Engineering*, 127, 433–444. doi: 10.1016/j.petrol.2015.01.040
[22] Wang, T., Yang, C., Ma, H., Daemen, J. J. K., & Wu, H. (2015b). Safety evaluation of gas storage caverns located close to a tectonic fault. *Journal of Natural Gas Science and Engineering*, 23, 281–293. doi: 10.1016/j.jngse.2015.02.005
[23] Wang, T., Yang, C., Ma, H., Li, Y., Shi, X., Li, J., & Daemen, J. J. K. (2016). Safety evaluation of salt cavern gas storage close to an old cavern. *International Journal of Rock Mechanics and Mining Sciences*, 83, 95–106. doi: 10.1016/j.ijrmms.2016.01.005
[24] Yang, C., Wang, T., Li, J., Ma, H., Shi, X., & Daemen, J. J. K. (2016). Feasibility analysis of using closely spaced caverns in bedded rock salt for underground gas storage: a case study. *Environmental Earth Sciences*, 75(15) 1138. doi: 10.1007/s12665-016-5944-3
[25] Yu, H., Liu, Y., Ma, H., Zhao, K., & Liu, J. (2022). Pillar safety in shallow salt caverns by using numerical simulations. *Journal of Energy Storage*, 55, 105881. doi: 10.1016/j.est.2022.105881
[26] Zhang, G., Wang, L., Wu, Y., Li, Y., & Yu, S. (2017). Failure mechanism of bedded salt formations surrounding salt caverns for underground gas storage. *Bulletin of Engineering Geology and the Environment*, 76(4), 1609–1625. doi: 10.1007/s10064-016-0958-3
[27] Zhang, G., Liu, Y., Wang, T., Zhang, H., Wang, Z., Zhao, C., & Chen, X. (2021). Pillar stability of salt caverns used for gas storage considering sedimentary rhythm of the interlayers. *Journal of Energy Storage*, 43, *103229*. doi: 10.1016/j.est.2021.103229
[28] Zhang, G., Liu, Y., Wang, T., Zhang, H., Wang, Z., & Zhao, C. (2022). Research on anchoring effect and failure mechanism of hard interlayers in the cavern pillar of underground gas storage in bedded salt formations. *Journal of Energy Storage*, 55, 105614. doi: 10.1016/j.est.2022.105614
[29] Zhang, N., Shi, X., Wang, T., Yang, C., Liu, W., Ma, H., & Daemen, J. J. K. (2017). Stability and availability evaluation of underground strategic petroleum reserve (SPR) caverns in bedded rock salt of Jintan, China. *Energy*, 134, 504–514. doi: 10.1016/j.energy.2017.06.073
[30] Zhang, N., Shi, X., Zhang, Y., & Shan, P. (2020). Tightness analysis of underground natural gas and oil storage caverns with limit pillar widths in bedded rock salt. *IEEE Access*, 8, 12130–12145. doi: 10.1109/ACCESS.2020.2966006